Preparation, characterization and sintering of yttrium-doped ThO2 for oxygen sensors applications

M. Gabard, Y. Cherkaski, L. Brissonneau, M. C Steil, J. Fouletier, Adel Mesbah, N. Dacheux, Nicolas Clavier

Preparation, characterization and sintering of yttrium-doped ThO_2 for oxygen sensors applications

M. Gabard [1,2,3], Y. Cherkaski [1,4], N. Clavier [4,], L. Brissonneau [1], M.C. Steil [2,3], J. Fouletier [2,3], A. Mesbah [4], N. Dacheux [4]*

[1] CEA/DEN/DTN/SMTA/LIPC, Site de Cadarache, 13108 St-Paul lez Durance, France

[2] Univ. Grenoble Alpes, LEPMI, F-38000 Grenoble, France

[3] CNRS, LEPMI, F-38000 Grenoble, France

[4] ICSM - UMR 5257, CEA/CNRS/ ENSCM/Univ. Montpellier, Site de Marcoule, BP 17171, 30207 Bagnols/Cèze cedex, France

*** Corresponding author :**

Dr. Nicolas CLAVIER
ICSM – UMR 5257 CEA/CNRS/UM/ENSCM
Site de Marcoule – Bât 426
BP 17171
30207 Bagnols sur Cèze
France

Phone : + 33 4 66 33 92 08
Fax : + 33 4 66 79 76 11

nicolas.clavier@icsm.fr

Abstract :

The preparation of $Th_{1-x}Y_xO_{2-x/2}$ ceramics, to be used as electrolyte in oxygen sensors for sodium-cooled nuclear reactors, was successfully undertaken from oxalate precursors. Such method was found to provide quantitative precipitation of the cations into $Th_{1-x}Y_x(C_2O_4)_2.2H_2O$ solid solutions up to x = 0.15 while a polyphase system was obtained for x = 0.22. The corresponding oxides were obtained through heat treatment in air at 500°C and characterized by the means of PXRD, SEM and statistical X-EDS measurements. The conditions for the densification of $Th_{1-x}Y_xO_{2-x/2}$ ceramics were further determined by dilatometry (T = 1575°C, t = 8 hours) resulting in densification rates up to 99%. Finally, a first estimation of the electric properties of the solids was undertaken by impedance spectroscopy. Electrical conductivity was found to increase linearly with the incorporation of Y^{3+} content while the associated values of activation energy decreased, with a minimum value of 1.1 eV for $Th_{0.85}Y_{0.15}O_{1.925}$.

Keywords : *yttria-doped thoria, synthesis, oxalate route, characterizations*

1. Introduction

In the framework of the development of the fourth generation of nuclear reactors, a Sodium-cooled Fast Reactor (SFR) is planned to be operated in France in the 2020's. In the primary vessels, the oxygen content in the liquid sodium coolant must be kept under a specific value (usually few ppm), as it controls the corrosion rate of the stainless steel claddings [1]. The oxygen content in the sodium is fixed by a cold trap, a component where a part of the sodium flow is deviated and oxygen precipitates as Na_2O when the saturation temperature is reached. A plugging indicator, associated to the cold trap, gives the total amount of impurity (susceptible to precipitate at low temperature) in the sodium. However, this device is not specific towards oxygen. In this context, the use of potentiometric sensors appears of great interest as it would bring a redundant, diversified and specific monitoring of the oxygen dissolved in sodium. In such sensors, the difference of oxygen activity in the sodium and in a reference induces a voltage drop according to Nernst's law. The reference and the sodium are separated by a solid electrolyte, which can be brazed on a metallic tube. The tightness between the outside and the inside of the sodium pipe is then easily performed on this metallic tube (the alternative being a long ceramic tube where tightness is performed *via* cooled sodium).

The quality of the electrolyte material is critical to insure the adequate operating of the sensors in the reactor environment [2]. It should be compatible with sodium at high temperature (about 400°C), mechanically resistant and a purely ionic conductor. In this context, the use of yttria-doped thoria (*i.e.* $Th_{1-x}Y_xO_{2-x/2}$) electrolyte was suggested ever since 1959 [3] for potentiometric sensors to be operated in liquid sodium. The incorporation of Y^{3+} in the fluorite-type structure of ThO_2 produces oxygen vacancies which turns the ceramic into an ionic conductor. Thoria is much less sensitive to sodium corrosion compared to zirconia, which was also frequently used in oxygen sensors [4]. Finally, one can achieve highly dense fine grains and high purity ceramic which is generally required to resist to sodium corrosion and mechanical stress [5].

The first potentiometric sensors dedicated to oxygen monitoring in sodiul were developed in the 1960's [6]. The electrolyte materials were generally based doped ThO_2 or ZrO_2, with metal/metal oxide or gas acting as reference electrode [7]. As instance, recent researches were conducted on Ca-doped [8] and Y-doped [9] zirconia because of the easier availability of the materials, but the best results were obtained with ThO_2-based solid

solutions [2, 3, 5-7, 10-18]. The majority of the probes produced up to now were designed in 1970's and 1980's, with some of them being tested in reactors [15, 17] and made commercially available. The yttrium incorporation ratio was usually in the 7.5-15 wt.% Y_2O_3 range, since the maximum ionic conductivity was reported for an yttrium doping of x = 0.15 [10, 18]. However, if lifetimes up to 10 000 hours were reported [11, 13] the probes generally suffered from their lack of robustness and reliability. Particularly, an important sensitivity to thermal and mechanical stress was observed and linked to a weakening of the probe both at the brazure level and within the ceramic electrolyte itself [14, 16]. Also, several authors underlined the crucial effect of the electrolyte purity over the probe performances. Indeed, the presence of impurities in the ceramic, and particularly within grain boundaries, was systematically associated to an increase of the corrosion rate in liquid sodium [19], and sometimes to the formation of secondary phases such as Na_2ThSiO_5 or Na_2SiO_5 at the surface of the electrolyte [12]. Nowadays, no more commercial oxygen sensors for sodium are available, and the sensor development is limited to few laboratories in India [8, 20], USA [9] and France.

New preparation routes for the $Th_{1-x}Y_xO_{2-x/2}$ electrolyte ceramic then have to be investigated in order to provide highly pure materials meeting the microstructural requirements detailed previously. For example, Cosentino *et al.* [21] chose a citrate technique, while Ganesan *et al.* [5] tried different methods, including citrate technique as well as Pechini and PEG-assisted processes. As a result, both obtained very fine grains powders and dense pellets. In this framework, oxalic co-precipitation can provide a suitable method for the elaboration of reliable and robust sensors [2]. Indeed, this preparation route is well-known to provide rapid and quantitative precipitation of tetravalent actinides [22, 23], and, after heat treatment, to yield powders with a high sintering capability [24, 25]. This paper is then dedicated to the synthesis of thorium(IV)-yttrium(III) mixed oxides through oxalic route, their complete physico-chemical characterization and the subsequent determination of sintering capability and evaluation of their electrical properties.

2. Experimental

2.1 Preparation of the precursors

All the chemical used during the preparation of the powdered samples, including thorium nitrate $Th(NO_3)_4.5H_2O$, were supplied by Sigma-Aldrich and were of analytical grade (purity ≥ 99%). Thorium-yttrium mixed oxalates were prepared following a protocol similar to that described by Horlait *et al.* [26], for $0.005 \leq x \leq 0.22$, with $x = Y/(Th+Y)$ is the cationic molar ratio. Thorium and yttrium nitrate salts were first dissolved in 1M HNO_3 in order to reach a final concentration in cations close to 0.5M. The two solutions were then mixed together in the desired stoichiometry then poured quickly in a beaker containing a large excess of oxalic acid. The precipitate instantaneously formed was further separated by centrifugation at 4500 rpm, washed several times with deionized water then ethanol, and then dried overnight in an oven at 90°C.

Precipitation yields were then determined through the analysis of the supernatant by ICP-AES measurements (Spectro Arcos EOP). Protocols for solution sampling and further ICP-AES analysis have been already described in one of our previous publication [27]. The emission bands chosen were 401.913, 283.730 and 274.716 nm for thorium, and 371.030 and 324.2278 nm for yttrium concentration determination.

2.2. Characterization of the solids

The powders obtained through the precipitation route described above were first characterized in terms of morphology. SEM observations were directly conducted on powdered samples without any preparation such as metallization, using a FEI Quanta 200 electronic microscope, equipped with an Everhart-Thornley Detector (ETD), in high vacuum conditions with a very low accelerating voltage (2 – 3.1 kV). These conditions were chosen in order to create a beam deceleration effect that led to high resolution images. For statistical X-EDS analyses, the powder was first embedded in an epoxy resin. The surface of the sample was then polished to reach an optical grade and covered by carbon coating. Experimental data were finally collected randomly from about 300 different locations of the sample surface, considering ThO_2 and YPO_4 as internal standards.

Powder X-Ray Diffraction (PXRD) patterns were obtained by the means of a Bruker D8 diffractometer equipped with a Lynx-eye detector adopting the parallel geometry (reflection mode) and using Cu $K\alpha_{1,2}$ radiation (λ = 1.54184 Å). PXRD patterns were recorded at room temperature in the $5° \leq 2\theta \leq 100°$ range, with a step size of $\Delta(2\theta) = 0.03°$ and a total counting time of about 1 hour. For *in situ* high temperature experiments, powders were placed in dedicated alumina boats and heated with a rate of 5°C.min^{-1}, under N_2 atmosphere. HT-PXRD patterns were recorded each 30°C from 30 to 300°C then each 50°C from 300 to 500°C and finally with a 100°C step from 500°C to 1000°C. Temperature was held for 15 minutes before recording the pattern in order to ensure the thermodynamic equilibration of the sample.

All the PXRD patterns were refined by the Rietveld method using the Cox-Hastings pseudo-Voigt profile function [28] implemented in the Fullprof_suite program [29]. During all the refinement, the conventional profile/structure parameters (zero shift, unit cell parameters, scale factors, global thermal displacement and asymmetric parameters) were allowed to vary. Moreover, for each phase, modelling of the intrinsic microstructure parameters was performed by applying an anisotropic size model.

Specific surface area measurements were determined using adsorption/desorption of N_2 at 77 K (BET method) by the means of a Micromeritics Tristar 3020 apparatus. Prior to the analyses, samples were outgassed at 90°C for 4 hours in order to ensure the release of water molecules adsorbed at the surface of the solids.

2.3. Thermal analyses and sintering

Dilatometric measurements were conducted on a Setaram Setsys Evolution apparatus. Heat treatments were carried out under air flux up to 1600°C with a rate of 10°C.min^{-1}. Dwell time of 30 minutes was then considered before sample was cooled down to room temperature at 30°C.min^{-1}.

In order to perform the sintering of thorium-yttrium oxides, the powdered samples by conversion of the oxalate precursors were first shaped by uniaxial pressing (500 MPa) at room temperature thanks to a Specac Atlas manual hydraulic press. The pellets obtained were then placed in alumina boats and heated up to 1575°C under air flow in a tubular furnace (Nabertherm). Heating rate of 10°C.min^{-1} was applied on heating, while natural cooling was used after sintering.

Finally, density measurements of the sintered pellets were conducted through two complementary techniques. Helium pycnometry analyses (Micromeritics Accupyc 1340) led to the contribution of the closed porosity while geometrical measurements using a precision calliper were further used to estimate the global porosity of the samples.

2.4. Electrical characterizations

After sintering, both sides of the pellets were covered by a platinum layer (Metalor 6082). The oxygen partial pressure in the experimental cell was controlled and monitored by means of a zirconia oxygen pump-sensor device (GEN'AIR, Setnag). Three samples can be characterized simultaneously enabling to compare the properties of pellets in the same conditions of temperature and oxygen partial pressure. The temperature of the samples was controlled within ± 1°C in the 350-800°C range. The electrical characterizations were carried out by impedance spectroscopy, using a Solartron SI1260 impedancemeter. The numbers in the diagrams indicate the logarithm of the measuring frequency.

3. Results and discussion

3.1 Characterization and conversion of oxalate precursors

Following the synthesis of oxalate precursors of thorium-yttrium oxides, the precipitation yields were first determined from ICP-AES measurements of the supernatant. Whatever the chemical composition considered, the precipitation of both cations appeared to be quantitative, with precipitation yields exceeding 99.8 % (**Table 1**), even if the concentration of yttrium in the supernatant always appeared to be higher than that of thorium. Additionally, the x molar ratio in the solid precipitated was also checked after the complete dissolution of an aliquot of oxalate powder in a mixture of concentrated HNO_3/HCl. Once again, the values obtained appeared in good agreement with the expected ones and confirmed the quantitative precipitation of the cations.

Table 1. Precipitation yields of thorium and yttrium determined from ICP-AES measurements for different x = Y/(Th+Y) mole ratios.

	x = 0.01		**x = 0.08**		**x = 0.15**		**x = 0.22**	
	Th	**Y**	**Th**	**Y**	**Th**	**Y**	**Th**	**Y**
Initial (mol.)	1.2×10^{-2}	1.2×10^{-4}	1.1×10^{-2}	9.6×10^{-4}	1.1×10^{-2}	1.8×10^{-3}	1.0×10^{-2}	2.8×10^{-3}
Soluble fraction (mol.)	4.3×10^{-8}	< L.D.	4.4×10^{-8}	2.0×10^{-7}	6.2×10^{-8}	1.4×10^{-6}	8.5×10^{-8}	4.9×10^{-6}
Precipitation yield (%)	> 99.99	> 99.9	99.99	99.98	99.99	99.92	99.99	99.82

L.D. : limit of detection

The morphology of the oxalate precursors was then evaluated thanks to SEM observations (**Figure 1**). For all the chemical composition studied (i.e. typically $0.005 \leq x \leq 0.22$), the powders appeared to be composed of rounded plate-like aggregates of about 1-2µm in length, themselves being composed by smaller submicrometric crystallites. This morphology is close to that already reported for thorium oxalate in the literature, frequently described as square-shaped agglomerates [25, 30, 31]. Also, the amount of Y^{3+} incorporated in the oxalate structure did not impact significantly the powders morphology since the grains size and the aggregation level appeared almost unchanged for all the samples studied.

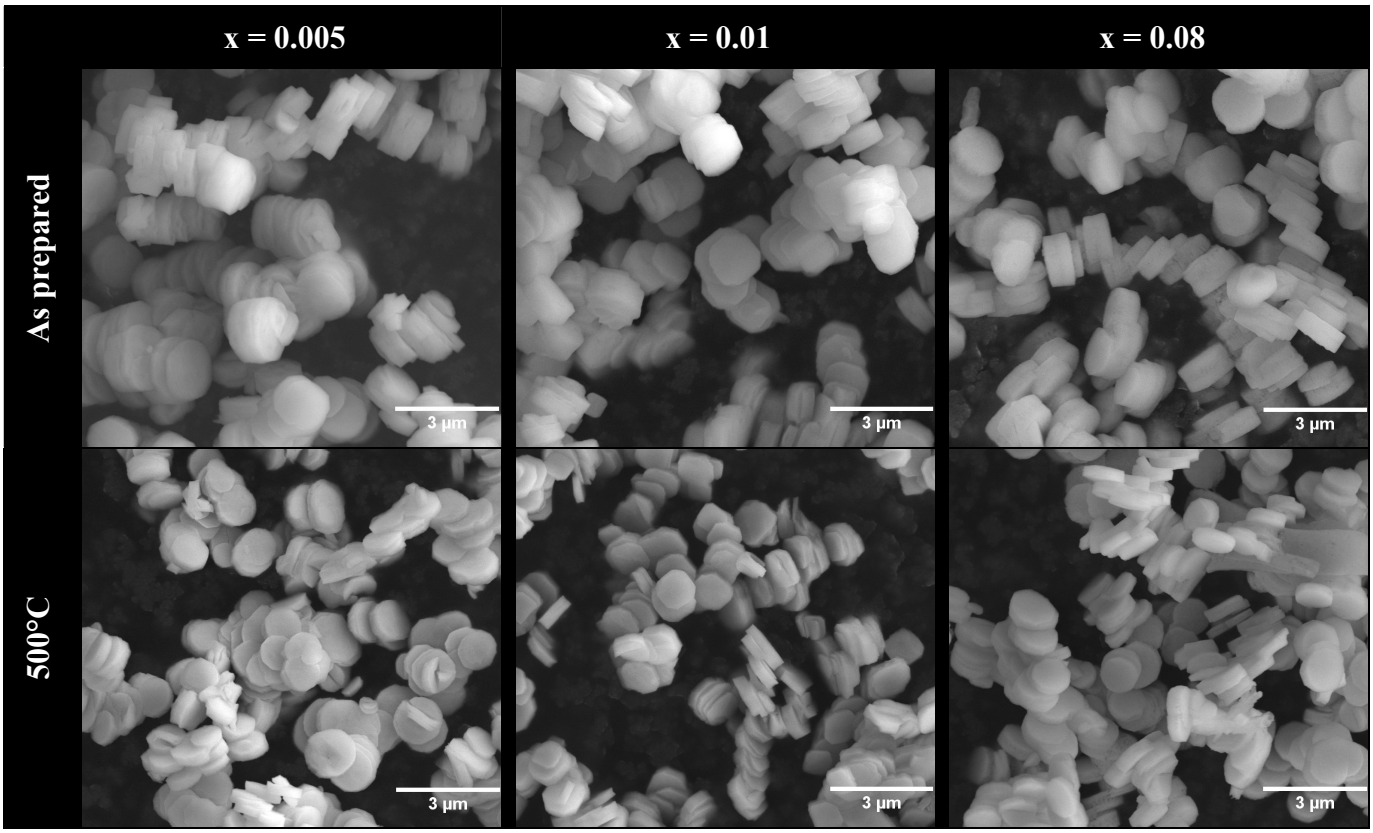

Figure 1. SEM observations of thorium-yttrium oxalates and corresponding mixed oxides prepared from the conversion of oxalate precursors at 500°C.

The powdered precursors prepared from oxalic co-precipitation of thorium and yttrium solutions were first investigated by the means of PXRD (**Figure 2a**). For yttrium amounts up to x = 0.15, the pattern recorded always appeared to fit with that already reported in the literature for thorium oxalate dihydrate (monoclinic, space group C2/c) [23]. The observation of a systematic and progressive shift of the PXRD lines toward the lower angles (as attested by the focus on the 15-18° range in the **Figure 2a**) accounts for the direct incorporation of yttrium within the thorium oxalate structure. Also, no evidence of $Y_2(C_2O_4)_3.nH_2O$ formation [32] was noted on the PXRD patterns. On this basis, one can conclude that the precipitation step yielded to the formation of $(Th,Y)(C_2O_4)_2.2H_2O$ solid solutions. Conversely, the sample prepared for x = 0.22 presented additional XRD lines assigned to the hexagonal structure (space group $P6_3/mmc$) already reported by Arab-Chapelet *et al.* for mixed An(IV)/Ln(III) or An(IV)/An(III) oxalates [33, 34]. Also, the position of the PXRD lines observed for this composition appeared to be closed to that noted for x = 0.15. The formation of a polyphase material can thus be associated to the existence of a limit of incorporation of Y^{3+} in the structure of $Th(C_2O_4)_2.2H_2O$ between 15 and 22 % in mole. This range of values appears in good agreement with the one previously evidenced by Horlait *et al.* during the study of

$(Th,Ln)(C_2O_4)_2.2H_2O$ compounds, as they ended up with polyphase systems for $x \geq 0.21$ whatever the trivalent lanthanide studied [26]. The existence of such incorporation limit, and the subsequent formation of polyphase oxalate precursor, are thus likely to create heterogeneities in the distribution of yttrium in the solid.

When heating (**Figure 2b**), the typical PXRD pattern recorded at room temperature was conserved up to 120°C: even if a phase transition toward an orthorhombic variety was reported around 110°C [23], the conditions of acquisition used for HT measurements hinder the detection of the slight pattern modifications associated. From 150°C, the apparition of additional peaks marked the progressive dehydration of the initial compound, first leading to $(Th,Y)(C_2O_4)_2.H_2O$ then to anhydrous $(Th,Y)(C_2O_4)_2$. These latter were unambiguously identified by analogy with the homologous thorium based compounds, namely $Th(C_2O_4)_2.H_2O$ and $Th(C_2O_4)_2$ [35].

Above 240°C, the intensity of the PXRD lines decreased strongly, indicating the progressive amorphization of the sample. Such decrease of the crystallization state was correlated with the decomposition of the oxalate entities, as already demonstrated in several other thorium-based chemical systems, such as Th-U(IV) [30] or Th-Ce(IV) [36] oxalates. For these types of compounds, the oxalate groups were found to be decomposed into CO and CO_2 gases in the 300-400°C range. In good agreement with these values, the characteristic pattern of the $Fm\bar{3}m$ fluorite-type structure of ThO_2 [37] was detected as soon as 400°C, even if the wide PXRD lines collected evidenced the poorly crystallized and/or the nanosized nature of the sample. The increase of temperature up to 900°C was then correlated with the narrowing of the PXRD lines, thus to the growth of the coherence domains [36].

(a)

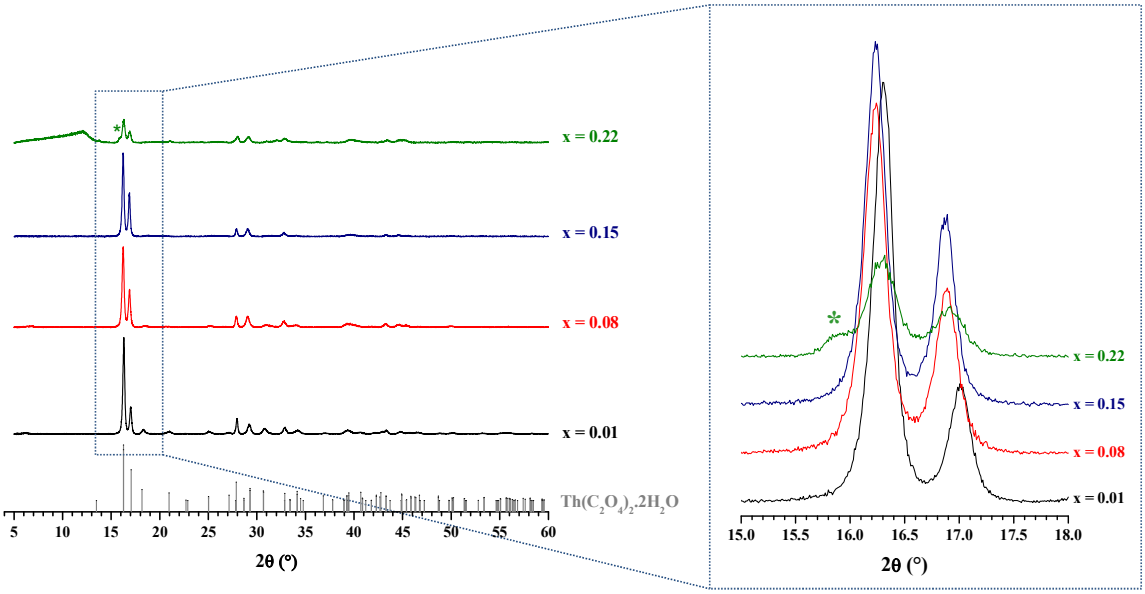

(b)

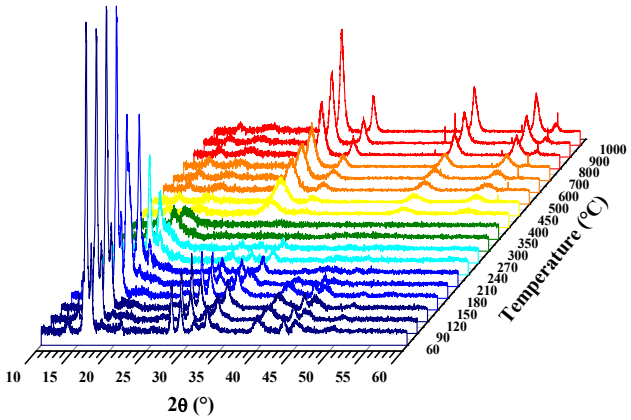

Figure 2. (a) PXRD patterns of $(Th,Y)(C_2O_4)_2.nH_2O$ precursors and comparison to $Th(C_2O_4)_2.2H_2O$, with detailed focus on the 15-18 ° range [23]. The star indicates additional phase for x = 0.22. (b) HT-PXRD monitoring of the conversion into dioxide for x = 0.08.

In parallel to the HT-XRD analyses, the variation of the powders specific surface area was also monitored versus the temperature of conversion. As expected from previous studies [38], the decomposition of the oxalate groups was associated with a strong increase in the specific surface area, leading to a maximum value after heating at 500°C. Such a modification in the topology of the powders could result either from the breakaway of the biggest aggregates during the emission of the gaseous species formed during the decomposition [39] or from the formation of mesopores of a few nanometers in diameter [36] due to the gas

release from and through the aggregates. Whatever the chemical composition considered, both these phenomena resulted in the increase of the specific surface area by about one order of magnitude.

Conversely, above 500°C, the specific surface dropped down significantly for all the three samples investigated. As reported previously, this tendency both arose from the crystallization of the samples (increase of the average crystallite size) and from the apparition of sintering phenomena (coalescence of agglomerates and grain growth) [40]. Owing to this potential loss of reactivity and to the early formation of the oxide structure, the operating conditions for the conversion of the oxalate precursors were then set to a heat treatment of 6 hours at 500°C under air atmosphere.

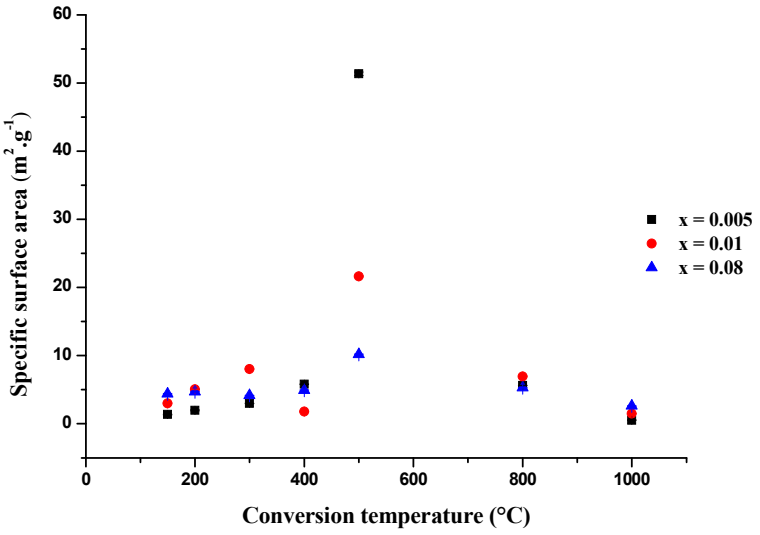

Figure 3. Variation of the specific surface area of $Th_{1-x}Y_x(C_2O_4)_2.2H_2O$ precursors versus temperature for x = 0.005 (■), x = 0.01 (●) and x = 0.08 (▲).

3.2 Characterization of the oxide samples

Thorium-yttrium mixed dioxides prepared from the conversion of the oxalate precursors at 500°C were first characterized by PXRD. As already evidenced from the high temperature data presented in **Figure 2b**, all the investigated samples presented the characteristic PXRD lines of the fluorite type structure. However, the important FWHM value of the PXRD peaks could be associated to the nanosized character of the samples and/or to an

heterogeneous distribution of yttrium in the ThO_2 structure. As a matter of fact, Rietveld refinement of the PXRD pattern (**Figure 4a**) revealed the existence of two distinct fluorite-type structures exhibiting close unit cell parameters (see red and blue calculated patterns in **Figure 4a** and associated unit cell parameters gathered in **Table 2**). Indeed, the experimental data could only be fitted with the contribution of at least two populations of PXRD peaks. The peaks exhibiting the highest 2θ values led to high values of unit volume, i.e. correspond to an yttrium-depleted phase owing to the respective ionic radii of Th^{4+} (1.19 Å) and Y^{3+} (1.159 Å) in the eight-fold coordination [41]. Such heterogeneity probably already existed within oxalate precursors and is likely to originate from differences in the precipitation kinetics of thorium(IV) and yttrium(III) in oxalic media.

Table 2. Data determined from Rietveld refinement of the XRD patterns of thorium-yttrium dioxides prepared after conversion of oxalate precursors at 600°C or 1400°C.

x	**0.005**	**0.01**	**0.08**	**0.15**	**0.22**
			$T_{conversion}$ = 600°C		
a_1 (Å)	5.5810(5)	5.5816(4)	5.5663(5)	5.5082(5)	5.5543(6)
a_2 (Å)	5.6128(4)	5.6145(3)	5.6046(4)	5.5761(3)	5.5964(6)
			$T_{conversion}$ = 1400°C		
a (Å)	5.5964(1)	5.5959(1)	5.5911(1)	5.5788(1)	5.5690(1)
$d_{calc.}$ ($g.cm^{-3}$)	9.98	9.95	9.58	9.24	8.88

Additional heat treatments followed by PXRD measurements were further performed up to 1600°C for the $Th_{0.92}Y_{0.08}O_{1.96}$ sample in order to monitor its homogenization. Indeed, the preparation of homogeneous samples at the submicrometric scale is a crucial point to ensure efficient ionic conductivity within the mixed oxides. Also, the determination of an homogenization temperature could act as a guideline to evaluate the sintering temperature to apply to prepare the final ceramic material. Up to 1200°C, the Rietveld refinement of the PXRD patterns systematically led to the determination of two distinct unit cell volumes (as illustrated by the shaded part of **Figure 4b**). However, their variation versus temperature revealed that they became closer and closer with increasing temperature. Such behaviour could be clearly assigned to the interdiffusion of cations in the system, leading to a progressive homogenization of the yttrium distribution in the structure. For the highest temperatures studied (i.e. 1400-1600°C), only one fluorite-type structure was pointed out

from PXRD data refinement, thus corresponding to an homogeneous $Th_{1-x}Y_xO_{2-x/2}$ solid solution.

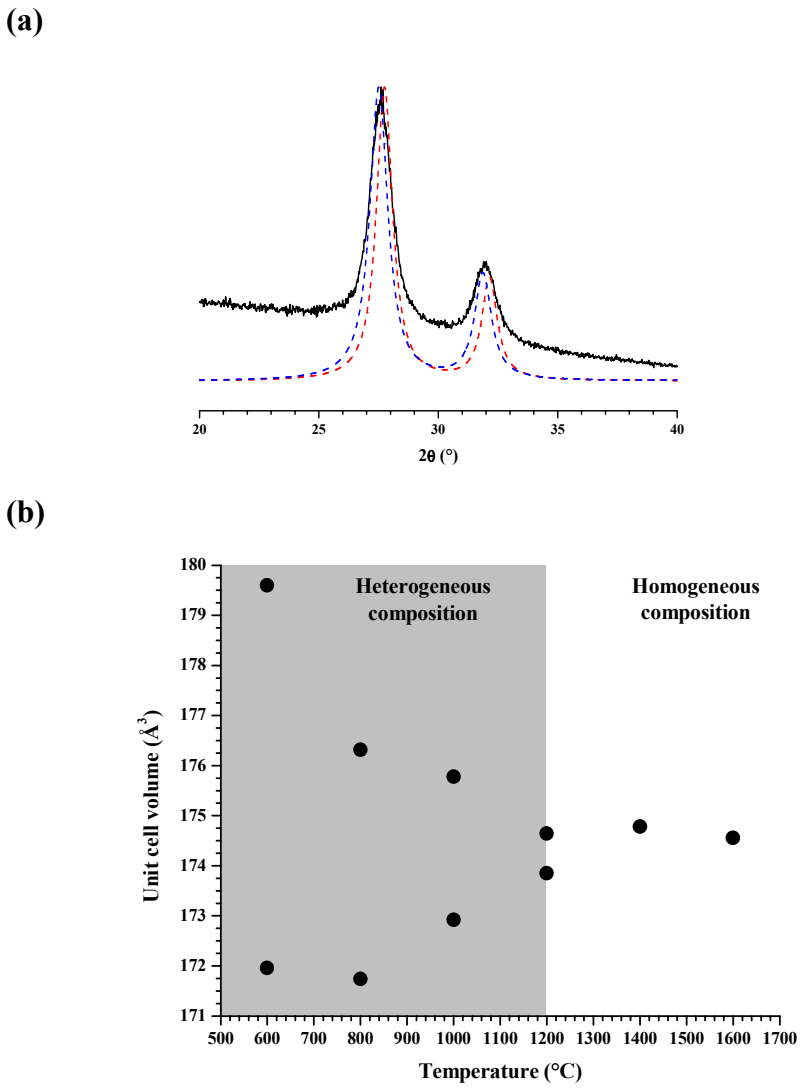

Figure 4. (a) Rietveld refinement of the PXRD data collected from $Th_{0.92}Y_{0.08}O_{1.96}$ after heating oxalate precursor at 500°C : black line stand for experimental data, while red and blue dashed lines account for calculated patterns. (b) Variation of the unit cell volumes versus heat temperature.

The unit cell parameters collected from samples heated at 1400°C show a continuous decrease versus x, in good agreement with the smaller ionic radius of Y^{3+} compared to Th^{4+} (**Table 2**, **Figure S1** supplied as supplementary material). This behaviour is in favour of the formation of a homogeneous solid solution at high temperature, even if the variation of the unit cell volume does not present a strictly linear trend with the yttrium content. Indeed,

Horlait *et al.* already demonstrated that such a variation obeys to a second-order polynom, as a result of the antagonist effects of the M^{3+} incorporation, on the one hand, and of the formation of oxygen vacancies that tend to decrease the O-O repulsion, on the other [26]. Also, it is to note that this result contrasts with that reported previously by Cosentino *et al.* [42] who described the variation of the unit cell parameter versus x as linear (**Figure S1**). However, they stated that a deviation from the standard Vegard law should occur and that the incorporation of yttrium in their samples might be incomplete. Also, the unit cell volumes determined in our study systematically appeared to be slightly higher than that reported by Cosentino *et al.* [42]. Such deviation could be linked with the co-precipitation method used to prepare our samples. Indeed, even when conducted in air, the conversion of oxalate precursors systematically leads to small amounts of residual carbon in the final oxide compounds (typically below 0.1 wt.%). Even if the exact location of carbon within the oxide structure was never clearly assessed, it was systematically associated to a slight swelling of the crystal lattice [43]. Nevertheless, the unit cell volumes determined in this work from the samples heated at 1400°C were considered as a reference and further used to determine the calculated density of the solids (**Table 2**).

The SEM observations performed on the oxide samples prepared after heating oxalate precursors at 500°C are gathered in **Figure 1**. From a general point of view, the morphological characteristics evidenced on the precursors were conserved on the oxide powders. Indeed, the grains conserved a general rounded-plates habit, even if their size slightly decreased. This modification, which is particularly noticeable on the grains thickness, could be directly linked with the dehydration then the decomposition of oxalate precursor. Nevertheless, the comparison between SEM observations of raw precursors and oxide samples still argue for a pseudomorphic conversion. This conservation of the general morphology was already stated for other compounds [39] and thus appears to be a characteristic of oxalate samples whatever the metallic cations considered.

Additionally, statistical X-EDS analysis were performed on the $Th_{0.85}Y_{0.15}O_{1.925}$ sample in order to quantify the heterogeneity of the yttrium distribution that was suggested from PXRD results. The statistical representation of the $x_{exp.}/x_{calc.}$ ratio (**Figure 5**) confirmed a non-homogeneous distribution of the yttrium in the ThO_2 structure. Moreover, it appears to follow a Gaussian law, with a Full Width at Half Maximum (FWHM) value of about 0.19. On this basis, and even if the average x ratio reached the expected value, the composition of the sample prepared for x = 0.15 was found to vary approximately between $Th_{0.82}Y_{0.18}O_{1.91}$ and

$Th_{0.88}Y_{0.12}O_{1.94}$. Nevertheless, such heterogeneity remains far below that what can be observed when proceeding through dry chemistry methods, i.e. mixture of pure powders. Indeed, no trace of pure ThO_2 or Y_2O_3 was detected neither from XRD nor EDS analyses. Also, from the XRD study, the samples were found to homogenize after heat treatment at high temperature ($T \geq 1400°C$). In these conditions, the small composition variation observed in the starting oxide powder could be expected to slightly delay the sintering step due to cation interdiffusion [44], but will not affect the properties of the ceramic, especially concerning ionic conduction.

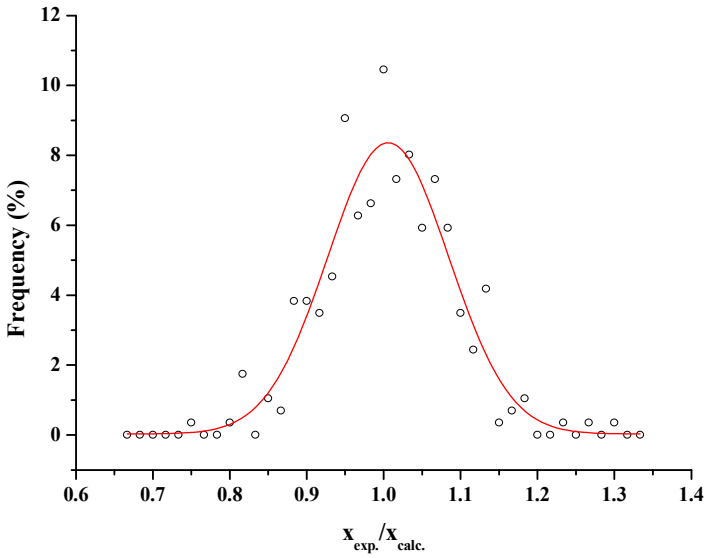

Figure 5. Statistical distribution of the Y/(Th+Y) mole ratio determined from EDS analysis of $Th_{0.85}Y_{0.15}O_{1.925}$.

3.3 Sintering of oxide samples

The sintering of the oxide samples obtained by firing oxalate precursors at 500°C was further investigated. In this aim, the powders were shaped by uniaxial pressing (500 MPa) at room temperature which resulted in pellets exhibiting a green density of about 50% whatever the yttrium content considered (**Table 3**).

Table 3. Relative density values determined for green and sintered $Th_{1-x}Y_xO_{2-x/2}$ pellets (T = 1575°C, t = 8 hours) from geometrical ($d_{geom.}/d_{calc.}$) and He-pycnometry ($d_{He}/d_{calc.}$) measurements with associated porosity distribution.

x	Green density (%)	$d_{geom.}/d_{calc.}$ (%)	$d_{He.}/d_{calc.}$ (%)	Open porosity (%)	Closed porosity (%)
0.005	55	95	95	0	5
0.08	49	99	99	0	1
0.15	48	97	98	1	2

Uncertainty attached to density measurements : ± 1%.
*$d_{calc.}$ values are given in **Table 2**.*

Dilatometric tests were then undertaken to determine the optimal conditions in terms of heating time and temperature required to reach the full densification of oxide samples. For all the yttrium contents investigated the relative shrinkage appeared to present similar variation versus temperature (**Figure 6a**). The densification proceeded through very progressive shrinkage with an onset between 500 and 600°C. Such temperature is obviously too low to be associated to sintering processes since full densification of ThO_2 is usually reported in the 1500-1700°C range in the literature [21, 24, 45, 46]. More likely, it could be assigned to the crystallite growth within the square-shaped agglomerates constituting the powder and/or to the elimination of residual carbon coming from the conversion of oxalate precursor. Indeed, Martinez *et al.* recently demonstrated that even small amounts of amorphous carbon (i.e. below 0.5 wt.%) could impact significantly the shrinkage of oxide powders prepared through oxalic co-precipitation method [43].

The shrinkage rate then appeared to increase when reaching higher temperatures, typically above 1300-1400°C. Even though, the relative linear shrinkage kept decreasing up to 1575°C, indicating that the sintering was incomplete at this latter temperature. On this basis, complementary experiments were run during an isotherm dwell of 8 hours at 1575°C (**Figure 6b**). For the three compositions studied, an additional shrinkage of about 2% was measured within the 6 first hours of heating. Based on the hypothesis of an isotropic shrinkage, such additional shrinkage should correspond to an increase in the densification of about 8% of the calculated density. In these conditions, a plateau of several hours at 1575°C appears to be compulsory in order to meet the requirements generally reported for electrolyte materials in oxygen sensors (i.e. $d_{geom.}/d_{calc.} \geq 97\%$).

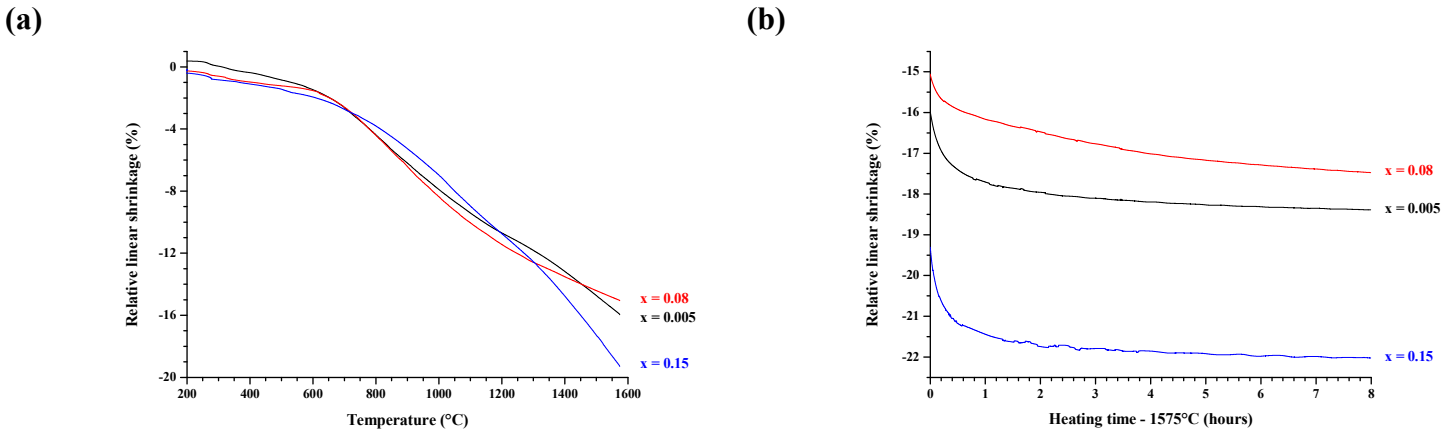

Figure 6. Variation of the relative linear shrinkage of $Th_{1-x}Y_xO_{2-x/2}$ solid solutions pellets versus temperature (a) and heating time at 1575°C (b).

The pellets collected after dilatometry tests were further analysed through geometrical and He-pycnometry measurements to estimate their relative density (**Table 3**). For all the samples, the density was found to be very high, *i.e.* above 95%. Such values thus confirmed that the densification process was almost fully achieved after heating 8 hours at 1575°C. Moreover, the comparison between geometrical and pycnometric data clearly showed that the remaining porosity was mainly constituted by closed pores, which is characteristic of the final step of the sintering. Nevertheless, due to the number of samples considered and to the uncertainty attached to the density measurements, it appeared impossible to conclude about the possible impact of the yttrium content on the final density of the pellets.

The good densification stated for all the samples was also confirmed by complementary SEM observations (**Figure 7**). Indeed, the micrograph recorded at the sample surface did not present any trace of porosity. Conversely, few pores were detected during the observation of a polished cross-section. They were found to be located in inter-granular position and then could probably be eliminated by prolonging the heat treatment. Also, a statistical analysis of the grain size was performed from several micrographs collected either from the surface or the bulk material. From this measurement, the grain size appeared to be typically distributed from 0.1 to 1.2 µm for the $Th_{0.92}Y_{0.08}O_{1.96}$ sample. The average grain size reached 0.45 µm and appeared to be homogeneous in the pellet, evidencing the absence of exaggerated grain growth at the surface. However, and as for the relative density values, it was not possible to establish a clear correlation between the average grain size and the yttrium content.

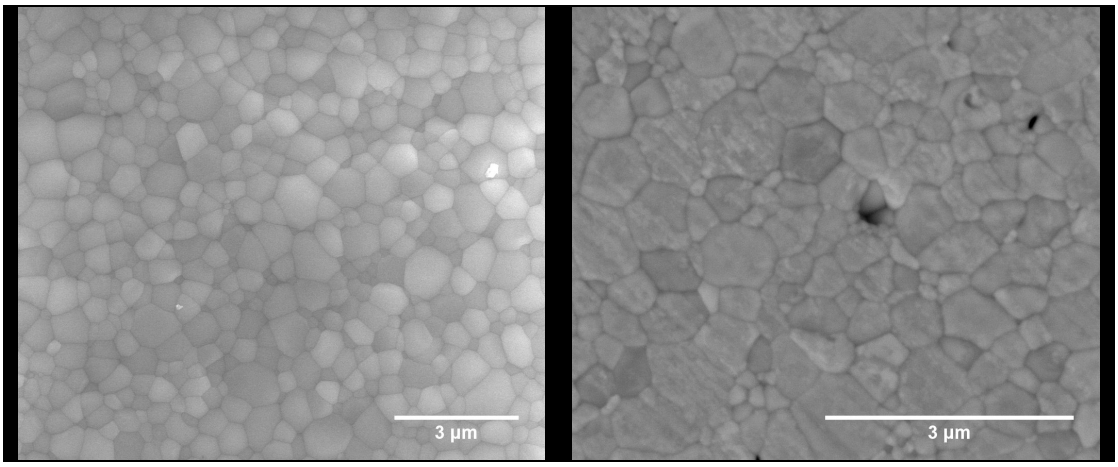

Figure 7. SEM observation of $Th_{0.92}Y_{0.08}O_{1.96}$ pellet after sintering at 1575°C during 8 hours : raw surface (left) and polished cross section (right).

3.4 Evaluation of the conducting properties

An example of impedance diagram obtained for the $Th_{0.095}Y_{0.08}O_{1.96}$ sample is presented in the **Figure 8** for experimental conditions corresponding to pure ionic conductor behaviour, i.e. at low oxygen partial pressure (10^{-6} bar). Three arcs were observed in the Nyquist representation, corresponding, in decreasing frequencies, to the bulk, the grain boundaries (referred to as G.B. in **Figure 8**), and the electrode contributions, respectively. The impedance diagrams were fitted with the ZView program. The bulk resistance (R_b) was determined from the intercept with the real axis of the high-frequency simulated arcs (frequencies higher than ca. 10^3-10^4 Hz according to temperature). In this paper, only the bulk contribution has been taken into account for the calculation of the electrical conductivity of the materials.

It has been shown previously that the thoria-doped oxides are mixed ionic-electronic conductor at high oxygen partial pressures with an additional p-type conductivity [10, 18]. However, for sufficiently doped materials, yttria-doped thoria exhibit a pure ionic conductivity under oxygen partial pressures lower than 10^{-5} bar. The aim of the preliminary study presented in this paper is to show the influence of the yttria content on the ionic conductivity. The variation of the electrical conductivity as a function of the oxygen partial pressure will be presented in a forthcoming publication.

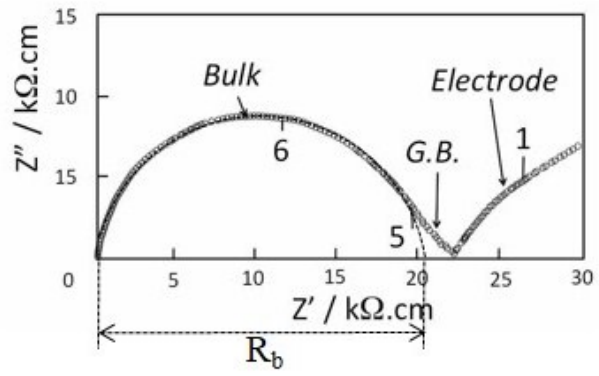

Figure 8. Typical impedance diagram obtained for $Th_{0.95}Y_{0.08}O_{1.96}$ sample (10^{-6} bar of oxygen, T = 500°C). The numbers in the diagram indicate the logarithm of the measuring frequency.

Figure 8 shows the variation of the conductivity as a function of the yttrium concentration, at 400°C (**Figure 9a**) and 800°C (**Figure 9b**). These results are compared to Hammou's work [10, 18].

(a) **(b)**

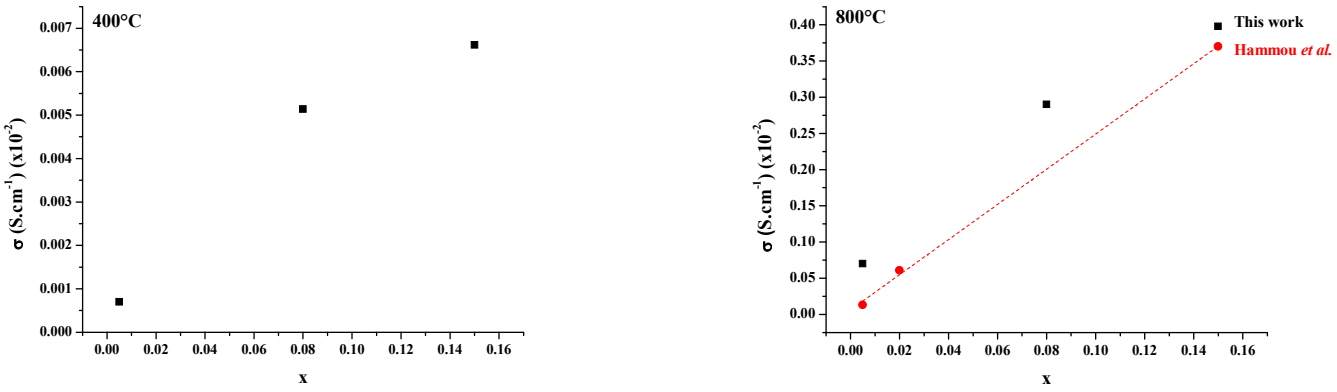

Figure 9. Variation of the electrical conductivity of $Th_{1-x}Y_xO_{2-x/2}$ compounds as a function of x, under 10^{-6} bar of oxygen, at 400°C (a) and 800°C (b) comparison with Hammou's works [10, 18].

The ionic conductivity varies linearly with the yttrium incorporation rate between x = 0 and x = 0.15. This phenomenon has been previously observed [10]. It should be pointed out that the lower conductivity observed by Hammou can be ascribed to differences in the purity of the oxide pellets used for the experiments and to some difficulties in the evaluation of the grain boundaries contribution.

Arrhenius plot of the bulk conductivity for three dopant levels, between 350 and 800°C, is reported in **Figure 10**. The activation energy of the electrical conductivity was 1.3 eV for $Th_{0.995}Y_{0.005}O_{1.9975}$ and 1.1 eV for $Th_{0.92}Y_{0.08}O_{1.96}$ and $Th_{0.85}Y_{0.15}O_{1.925}$. The activation energy decreases as a function of the dopant concentration. This is consistent with the results reported in literature, showing that the activation energy exhibits a minimum value for a composition close to x = 0.15 [10].

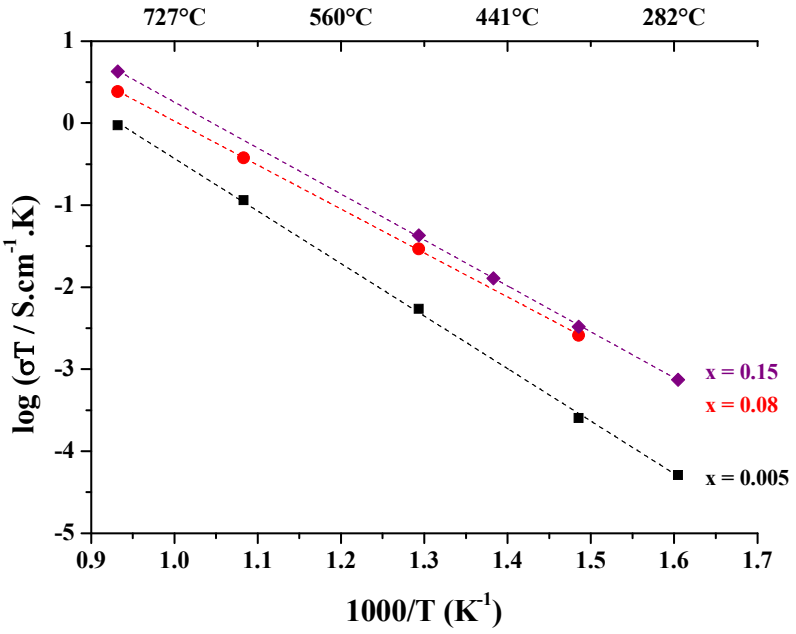

Figure 10. Arrhenius plot of the bulk conductivity of $Th_{1-x}Y_xO_{2-x/2}$ samples, for various dopant levels, under 10^{-6} bar of oxygen.

5. Conclusion

Pure $Th_{1-x}Y_xO_{2-x/2}$ ceramics, aimed to be used as electrolyte material in oxygen sensors, were successfully obtained from the conversion of oxalate precursors at 500°C. Such wet-chemistry route ensured the rapid and quantitative precipitation of the cations into $Th_{1-x}Y_x(C_2O_4)_2.2H_2O$ solid solutions. Nevertheless, a statistical EDS study coupled to XRD measurements revealed that the distribution of the cations in the samples remained slightly heterogeneous, probably as a consequence of differences in the precipitation kinetics of thorium(IV) and yttrium(III).

The conditions leading to the full densification of $Th_{1-x}Y_xO_{2-x/2}$ ceramics were thereafter determined by dilatometry and set to a heat treatment of 8 hours at 1575°C. Such operating conditions led to relative densities up to 99%, associated to a fine-grains microstructure, in good agreement with the specifications generally required for electrolyte material in oxygen sensors to be used in liquid sodium.

Finally, a very first estimation of the electric properties of the samples was undertaken by impedance spectroscopy. Electrical conductivity was found to increase linearly up to x = 0.15 with the incorporation of trivalent yttrium in ThO_2, in good agreement with the formation of oxygen vacancies. Accordingly, a decrease in the associated values of the activation energy was observed.

Additional experiments are now under progress to get a better understanding on both sintering behavior and electrical properties. On the one hand, the influence of the yttrium content on the final microstructure of the pellets will be evidenced, based on the establishment of sintering maps. On the other hand, complementary impedance spectroscopy measurements should allow to point out the relative contributions of grains and grains boundaries in the global electrical conductivity of the samples.

Acknowledgements

Authors would like to thank Johann Ravaux (ICSM/L2ME) for performing SEM observations. They are also grateful to the TECNA project of CEA for its continuous financial support.

Supplementary data

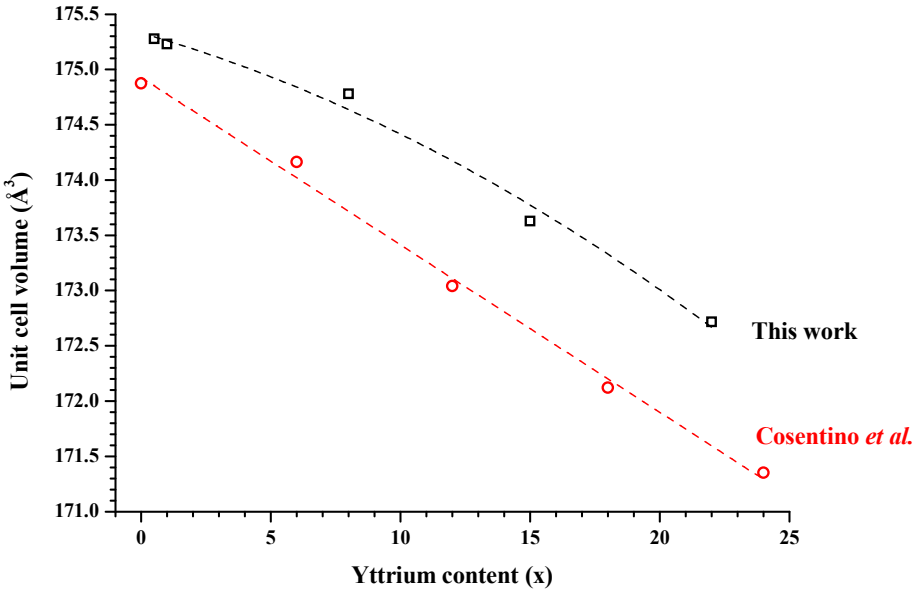

Figure S1. Variation of the unit cell volume of $Th_{1-x}Y_xO_{2-x/2}$ solid solutions versus x, and comparison with the results reported by Cosentino *et al*. [42]. XRD measurements were conducted at room temperature on samples previously heated for 6 hours at 1400°C (this study) or 2 hours at 1550°C [42].

References

[1] L. Brissonneau, New considerations on the kinetics of mass transfer in sodium fast reactors: An attempt to consider irradiation effects and low temperature corrosion, J. Nucl. Mater., 423 (2012) 67-78.

[2] R. Thompson, R.G. Taylor, R.C. Asher, C.C.H. Wheatley, R. Dawson, Experience of the production, performance and application of harwell oxygen meter tubes, in: Proc 2nd Int Conf on Liquid Metal Technol, Richland, USA, 1980, pp. 16-19.

[3] D.J. Hayes, Instrumentation for Liquid-Sodium in Nuclear-Reactors, J Phys E Sci Instrum, 7 (1974) 69-75.

[4] R.G. Taylor, R. Thompson, Testing and Performance of Electrolytic Oxygen Meters for Use in Liquid-Sodium, J Nucl Mater, 115 (1983) 25-38.

[5] R. Ganesan, S. Vivekanandhan, T. Gnanasekaran, G. Periaswami, R.S. Srinivasa, Novel approach for the bulk synthesis of nanocrystalline yttria doped thoria powders via polymeric precursor routes, J. Nucl. Mater., 325 (2004) 134-140.

[6] B. Minushkin, Plugging meter and continuous oxygen meter, in, United Nuclear Corporation, White Plains, NewYork, 1964.

[7] J.M. Mckee, D.R. Vissers, P.A. Nelson, B.R. Grundy, E. Berkey, G.R. Taylor, Calibration Stability of Oxygen Meters for Lmfbr Sodium Systems, Nucl Technol, 21 (1974) 217-227.

[8] K. Chandran, P. Muralidaran, D. Saisubalakshmi, V. Ganesan, Performance testing of in-sodium sensors and simulated experiments in, sodium chemistry loop, Nucl. Eng. Des., 268 (2011) 1-9.

[9] B.K. Nollet, Electrochemical Oxygen Sensor Development for Liquid Sodium, PhD Thesis, University of Wisconsin, 2013.

[10] A. Hammou, Mécanismes de conduction électrique dans les solutions solides à base de dioxyde de thorium, State Thesis, Université de Grenoble, 1973.

[11] M.R. Hobdell, C.A. Smith, Electrochemical Techniques for Monitoring Dissolved Carbon, Hydrogen and Oxygen in Liquid-Sodium, J. Nucl. Mater., 110 (1982) 125-139.

[12] D. Jakes, J. Kral, J. Burda, M. Fresl, Development of Electrochemical Oxygen Meter for Liquid-Sodium, Solid State Ionics, 13 (1984) 165-173.

[13] J. Jung, Oxygen Determination in Liquid-Sodium with Industrial Electrochemical Measuring Probe, J. Nucl. Mater., 56 (1975) 213-220.

[14] F.A. Kozlov, E.K. Kuznetsov, T.A. Vorobeva, K. Ulmann, T. Reetts, V. Rikhter, Electrochemical-Cell for Measuring the Activity of Oxygen in Sodium, Sov Atom Energy+, 51 (1981) 516-519.

[15] L. Mason, N.S. Morrison, C.M. Robertson, The monitoring of oxygen, hydrogen and carbon in the sodium circuits of the PFR, in: Liquid Metal Engineering and Technology, Oxford, 1984, pp. 53-59.

[16] J.M. Mckee, F.A. Smith, E.R. Koehl, Sodium-Hydroxide Injections into Sodium, T Am Nucl Soc, 33 (1979) 264-265.

[17] M.M. Osterhout, Operating experience with on-line meters at experimental breeder reactor II (EBR II), in: Proc 2nd Int Conf on Liquid Metal Technol, Richland, USA, 1980, pp. 9-15.

[18] E. Schouler, A. Hammou, M. Kleitz, Complex Impedance of Electrochemical Cells Based on Yttria Doped Thoria, Mater Res Bull, 11 (1976) 1137-1146.

[19] H.S. Isaacs, Calibration of oxygen meters in sodium using uranium, J Electrochem Soc, 119 (1972) 455-459.

[20] R. Ganesan, V. Jayaraman, S.R. Babu, R. Sridharan, T. Gnanasekaran, Development of Sensors for On-Line Monitoring of Nonmetallic Impurities in Liquid Sodium, J. Nucl. Sci. Technol., 48 (2014) 483-489.

[21] I.C. Cosentino, R. Muccillo, Powder synthesis and sintering of high density thoria-yttria ceramics, J Nucl Mater, 304 (2002) 129-133.

[22] F. Abraham, B. Arab-Chapelet, M. Rivenet, C. Tamain, S. Grandjean, Actinide oxalates, solid state structures and applications, Coord. Chem. Rev., 266-267 (2014) 28-68.

[23] N. Clavier, N. Hingant, M. Rivenet, S. Obbade, N. Dacheux, N. Barre, F. Abraham, X-Ray Diffraction and μ-Raman Investigation of the Monoclinic-Orthorhombic Phase Transition in $Th_{1-x}U_x(C_2O_4)_2 \cdot 2H_2O$ Solid Solutions, Inorg Chem, 49 (2010) 1921-1931.

[24] K. Ananthasivan, S. Anthonysamy, A. Singh, P.R. Vasudeva Rao, De-agglomeration of thorium oxalate-a method for the synthesis of sinteractive thoria, J Nucl Mater, 306 (2002) 1-9.

[25] G.D. White, L.A. Bray, P.E. Hart, Optimization of Thorium Oxalate Precipitation Conditions Relative to Derived Oxide Sinterability, J Nucl Mater, 96 (1981) 305-313.

[26] D. Horlait, N. Clavier, N. Dacheux, R. Cavalier, R. Podor, Synthesis and characterization of $Th_{1-x}Ln_xO_{2-x/2}$ mixed-oxides, Mater Res Bull, 47 (2012) 4017-4025.

[27] D.T. Costin, A. Mesbah, N. Clavier, S. Szenknect, N. Dacheux, C. Poinssot, J. Ravaux, H.P. Brau, Preparation and characterization of synthetic $Th_{0.5}U_{0.5}SiO_4$ uranothorite, Progress in Nuclear Energy, 57 (2012) 155-160.

[28] P. Thompson, D.E. Cox, J.B. Hastings, Rietveld refinement of Debye-Scherrer synchrotron X-ray data from Al_2O_3, Journal of Applied Crystallography, 20 (1987) 79-83.

[29] C. Frontera, J. Rodriguez-Carvajal, FullProf as a new tool for flipping ratio analysis, Physica B: Condensed Matter, 335 (2003) 219-222.

[30] N. Hingant, N. Clavier, N. Dacheux, N. Barre, S. Hubert, S. Obbade, F. Taborda, F. Abraham, Preparation, sintering and leaching of optimized uranium thorium dioxides, J Nucl Mater, 385 (2009) 400-406.

[31] G. Heisbourg, S. Hubert, N. Dacheux, J. Ritt, The kinetics of dissolution of $Th_{1-x}U_xO_2$ solid solutions in nitric media, J Nucl Mater, 321 (2003) 141-151.

[32] S. Balakrishnan, K. Ananthasivan, K.C.H. Kumar, Studies on the synthesis of nanocrystalline yttria powder by oxalate deagglomeration and its sintering behaviour, Ceramics International, 41 (2015) 5270-5280.

[33] B. Arab-Chapelet, S. Grandjean, G. Nowogrocki, F. Abraham, Synthesis and characterization of mixed An(IV)An(III) oxalates (An(IV) = Th, NP, U or Pu and An(III) = Pu or Am), J Nucl Mater, 373 (2008) 259-268.

[34] E. Brackx, J.P. Laval, O. Dugne, J.P. Feraud, B. Arab-Chapelet, Structural study of $(N_2H_5,H)_{2.9}U_{1.1}Ce_{0.9}(C_2O_4)_5 . 10H_2O$ from a conventional X-ray diffraction diagram obtained on a powder synthesized by a fast vortex process, J Solid State Chem, 221 (2015) 166-172.

[35] S. Dash, R. Krishnan, M. Kamruddin, A.K. Tyagi, B. Raj, Temperature programmed decomposition of thorium oxalate hexahydrate, J Nucl Mater, 295 (2001) 281-289.

[36] L. Claparede, N. Clavier, N. Dacheux, A. Mesbah, J. Martinez, S. Szenknect, P. Moisy, Multiparametric Dissolution of Thorium-Cerium Dioxide Solid Solutions, Inorg Chem, 50 (2011) 11702-11714.

[37] K. Clausen, W. Hayes, J.E. Macdonald, P. Schnabel, M.T. Hutchings, J.K. Kjems, Neutron scattering investigation of disorder in UO_2 and ThO_2 at high temperatures, High Temp. - High Press., 15 (1983) 383-390.

[38] D. Dollimore, The Thermal-Decomposition of Oxalates - a Review, Thermochim Acta, 117 (1987) 331-363.

[39] N. Hingant, N. Clavier, N. Dacheux, S. Hubert, N. Barre, R. Podor, L. Aranda, Preparation of morphology controlled $Th_{1-x}U_xO_2$ sintered pellets from low-temperature precursors, Powder Technol, 208 (2011) 454-460.

[40] L. Claparede, N. Clavier, N. Dacheux, P. Moisy, R. Podor, J. Ravaux, Influence of Crystallization State and Microstructure on the Chemical Durability of Cerium-Neodymium Mixed Oxides, Inorg Chem, 50 (2011) 9059-9072.

[41] R.D. Shannon, Revised Effective Ionic-Radii and Systematic Studies of Interatomic Distances in Halides and Chalcogenides, Acta Crystallogr A, 32 (1976) 751-767.

[42] I.C. Cosentino, R. Muccillo, Lattice parameters of thoria-yttria solid solutions, Mater Lett, 48 (2001) 253-257.

[43] J. Martinez, N. Clavier, T. Ducasse, A. Mesbah, F. Audubert, B. Corso, N. Vigier, N. Dacheux, From uranium(IV) oxalate to sintered UO_2: Consequences of the powders' thermal history on the microstructure, J Eur Ceram Soc, 35 (2015) 4535-4546.

[44] M.T. Aybers, Analysis of the Initial-Stage of Oxide Sintering - $(U_{0.8}Th_{0.2})O_{2+x}$, $(U_{0.2}Th_{0.8})O_{2+x}$, $(U_{0.05}Th_{0.95})O_{2+x}$, J Nucl Mater, 226 (1995) 27-33.

[45] Jorgense.Pj, W.G. Schmidt, Final Stage Sintering of ThO_2, J Am Ceram Soc, 53 (1970) 24-27.

[46] T.R.G. Kutty, K.B. Khan, P.V. Hegde, J. Banerjee, A.K. Sengupta, S. Majumdar, H.S. Kamath, Development of a master sintering curve for ThO_2, J Nucl Mater, 327 (2004) 211-219.